FOR COMMERCIAL RELEASE
PROPRIETARY INFORMATION
HAS BEEN DELETED

TECHNICAL MEMORANDUM
EERO/TM-70-11



# SUMMARY OF UNDERWATER CRATERING TESTS CONDUCTED AT SITE 300 DURING 1970



Prepared by
Kenneth T. Sakai
Robert F. Bourque

U. S. Army Engineer Explosive Excavation Research Office
(Lawrence Livermore Laboratory, Livermore, California)

An Activity of the
U. S. Army Engineer Waterways Experiment Station
(Vicksburg, Mississippi)

August 1971



407203

## ABSTRACT

Laboratory tests were conducted to determine the effect of a water overburden on cratering performance in sand. The objectives were to determine the parameters which describe the effect of the water overburden on the final crater configuration and to develop a relationship for the maximum water wave generated by the explosion. Spherical one-pound charges of composition C-4 were detonated at depths of burial in the medium ranging from 0 to 24 inches with a varying water overburden of 0 to 12 inches. Crater dimensions and maximum wave height data were analyzed empirically with the Buckingham Pi dimensional analysis technique. The data indicate that crater dimensions appear to be sensitive to small changes in water overburden (d) for a constant depth of burial in the medium ($d_m$) for $0<\frac{d}{d_m}<0.6$. The most sensitive region is $0<\frac{d}{d_m}<0.2$, where the crater radius increases abruptly, the crater depth decreases sharply, and the lip height decreases as the water depth is increased. The parameters which scale the maximum wave height, H, are $\frac{Hr}{d^2}$ and $\frac{Z d^3}{W}$, where r is the radial distance from the explosive, Z is the lithostatic head on the explosive charge, and W is the weight of the charge.


Per agreement
BG-0167A (a thru f)



A

## TABLE OF CONTENTS

## LIST OF TABLES AND FIGURES

List of Figures, continued

## LIST OF SYMBOLS

| | |
|---|---|
| $d$ | depth of water at surface zero |
| $d_m$ | depth of burial in the cratering medium |
| $g$ | gravitational acceleration |
| $\rho$ | density of water |
| $\rho_m$ | density of the cratering medium |
| $r$ | horizontal distance from surface ground zero |
| $z$ | confining overburden pressure on the charge |
| $E$ | total explosive energy |
| $H$ | maximum wave height measured from crest to following trough |
| $L$ | characteristic length |
| $Q$ | explosive energy released per unit weight of the charge |
| $V$ | volume of the apparent crater |
| $W$ | total weight of the charge |
| $Z$ | lithostatic head on the charge |

# SUMMARY OF UNDERWATER CRATERING TESTS CONDUCTED AT SITE 300 DURING 1970

## 1. Introduction

### Purpose

This laboratory-scale experiment was conducted at the Lawrence Livermore Laboratory High Explosive Test Facility (Site 300) near Tracy, California from December 1969 to May 1970 by the Explosive Excavation Research Office in order to determine the effect of a water layer on cratering in a cohesionless, homogeneous medium. The primary objective was to determine the laws of similitude which describe the effect of the water overburden on the final configuration of the apparent crater. A secondary objective was to develop a scaled relationship for the maximum surface water wave generated by the explosion.

### Scope

This study used single, one-pound charges of composition C-4 detonated at various depths of burial in sand with varying depths of water overburden to define the scaling parameters for underwater cratering. The depths of burial varied from 0 to 24 inches while the water overburden varied from 0 to 12 inches. A total of 81 cratering tests were performed.

### Background

Previous studies of underwater explosions were related to the destructive capabilities of a nuclear device detonated underwater near strategic military targets. These studies were concerned with the destructive potential of the airblast, ground shock, water shock, and surface water waves. In most cases, the charge was positioned at or above the seafloor. These studies consisted of both large- and small-scale testing with chemical

explosives as well as with several nuclear devices. Davis and Rooke[1] presents data of underwater craters formed by chemical explosives detonated at the seafloor. Van Dorn, et al.,[2] presents a compilation of water waves generated by charges detonated in the water layer.

Probably the first comprehensive experiment where the charges were buried beneath the seafloor was conducted by the Waterways Experiment Station in the early 1950's[3]. The objective of this program was to develop a technique to predict the destructive capability of a 20-kiloton nuclear device in water depths typical of most harbors. Scaling relationships for crater dimensions, maximum wave heights, airblast, water shock, and ground shock were developed with TNT charges ranging from 0.5 to 2048 pounds. Predictions of the destructive effects for a 20-kiloton device were made by scaling with these relationships up to the high yield range.

The only recent data comes from Project TUGBOAT, a large-scale underwater cratering experiment conducted by the U. S. Army Nuclear Cratering Group (now the Explosive Excavation Research Office ) in 1970[4, 5]. A small boat harbor was created by a series of twelve 10-ton charges of aluminized ammonium nitrate slurry detonated at a depth of about 36 feet in the coral. The water depths above the charges varied from 5 to 8 feet.

The Site 300 underwater cratering tests originated with the concept of using explosive excavation techniques to construct a deep draft harbor. The model testing would determine if the final crater configuration is practical for a deep draft harbor and also reveal design problems that may arise.

## 2. Experimental Procedure

### Description of the Test Facility

The underwater cratering tests were conducted at the indoor test pit, Bunker 804, Site 300. This test pit measures 60 feet by 30 feet and has an

average depth of 5 feet. It is equipped with a rolling bridge which is used to grade the surface of the cratering medium and to serve as a working platform for post shot surveys. The pit is sheltered by a steel frame structure with movable canvas roof panels to control the lighting for photography.

The existing test pit was waterproofed with a vinyl membrane and backfilled with sand to a depth of 4 feet. A wooden freeboard 1 foot high was constructed around the pit to support the membrane and to maintain a water level above the ground level of the pit. The final dimensions of the pit after modifications were 60 feet by 20 feet. A cross-sectional view of the modified test pit is shown in Figure 1.

The test pit was filled to the desired water level with a fire hose and drained with a water pump. The sides of the pit were lined with 2-inch-thick rubberized horsehair which effectively damped the water waves generated by the explosion and minimized wave reflection.

Description of Explosive Charges

The chemical explosive used in this test series was composition C-4, a plastic explosive with a TNT equivalence of 1.3. One pound of the explosive was molded into a spherical plastic shell and center initiated with a SE-1 detonator.

The emplacement hole was dug by hand auger to the required depth of burial, the charge was emplaced, and the hole was backfilled with sand. The pit was then filled with water to the desired depth.

Description of Wave Gages

The surface water waves generated by the explosion were recorded with two variable resistance gages and a Tektronix 502A oscilloscope. The wave gages were constructed of two parallel stainless steel rods 1/4 inch in diameter, 30 inches long, and spaced 1-1/4-inches apart. The two rods

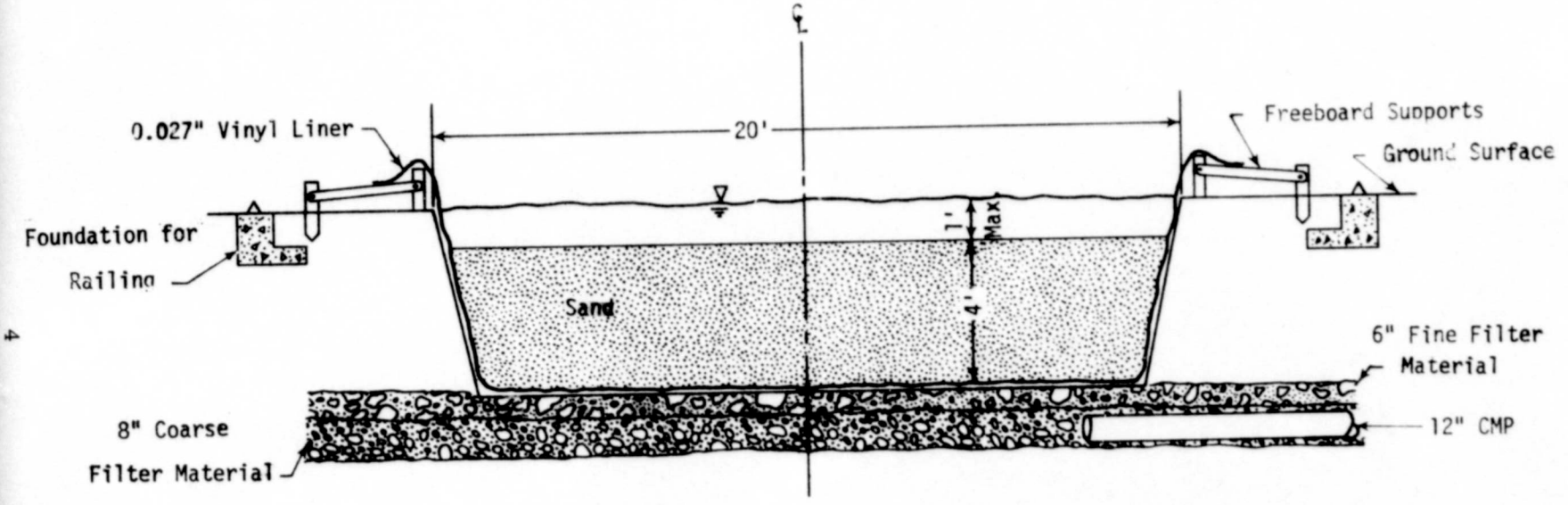


Figure 1. Cross Section of Modified Test Pit, Bunker 804, Site 300

were mounted vertically on a 1/2-inch-thick rectangular lucite pad. The top of the pad was buried flush with the sand and four galvanized spikes driven through the pad were used as anchors. Construction details and the electronic circuit diagram for the wave gages are shown in Figure 2.

The Tektronix 502A dual beam oscilloscope allows the inputs from two sources to be displayed on its screen. The fluctuation of the water surface as the wave passes the wave gage is electronically converted into a corresponding fluctuating voltage across the input terminals of the oscilloscope. The wave is then traced on the screen at a pre-selected amplitude and time scale. The screen display is photographed with a special Tektronix camera using Polaroid film.

Technical Programs

The technical programs conducted during these tests included crater measurements, surface water wave measurements, and high-speed documentation of the mound growth, wave propagation, and washback.

Profiles of the resultant craters were taken along two orthogonal axes. Crater elevations were taken at half-foot intervals. Crater dimensions were determined directly from these surveys.

The surface waves were recorded with two surface profile gages. The water displacements were traced on the screen of a Tektronics 502A oscilloscope and the traces were photographed with Polaroid film. The wave amplitudes and wave travel times were obtained directly from the photographic record.

High-speed photography was used to document the mound and plume growth, venting of the mound, propagation of the explosion-generated wave, and the washback and disintegration of the crater. This documentation

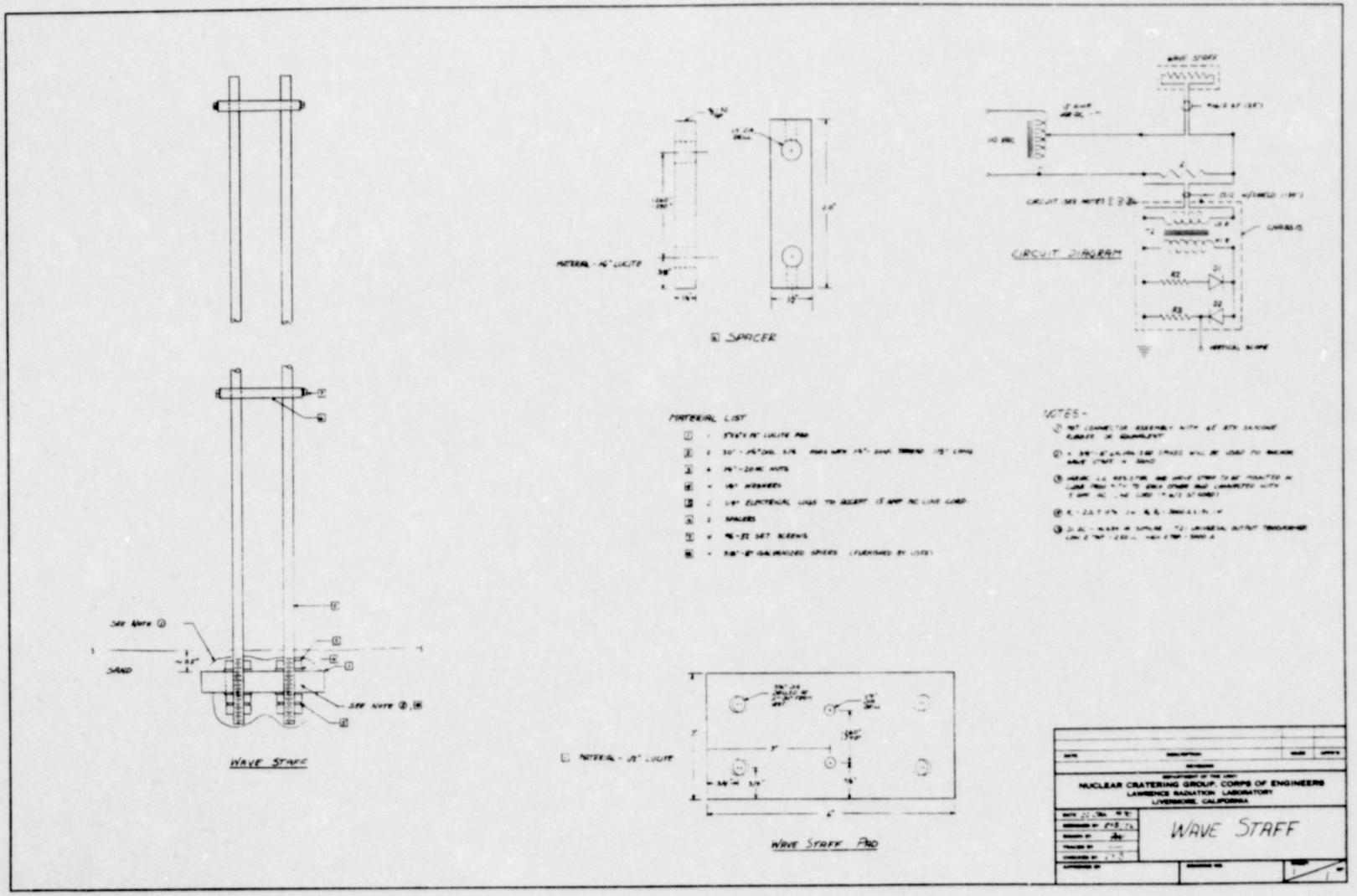


Figure 2. Wave Gage Details

provided an excellent visual account of the underwater cratering phenomenon. However, in most cases, the post-detonation history was screened by the dust cloud and qualitative data could not be obtained.

## 3. Experimental Results

### Underwater Cratering

The cratering curves for this experiment were developed by use of the CRATER DATA Code, a Fortran program for the Control Data Corporation 6600 Computer[6]. This code takes certain crater dimensions from the postshot profiles of each shot and computes apparent crater volume, average lip radius and height, average apparent radius, and apparent depth. Each of these variables is plotted as a function of depth of burial for a given water depth on a cartesian plane and a quadratic least squares fit is generated through the data points.

Cratering curves for apparent crater volume, apparent crater radius, apparent crater depth, and apparent lip height as a function of depth of burial in the medium for constant water depths of 0, 1, 2, 4, 8, and 12 inches are shown in Figures 3 through 10. For each constant water depth, the depths of burst tested were 0, 6, 12, 13, 17, 20 and 24 inches. A majority of the shots were repeated to check the reproducibility of the underwater craters.

### Explosion-Generated Water Waves

The two wave gages were installed 7 and 8 feet on a radial line from Ground Zero. A typical wave record is shown in Figure 11. The upper wave profile is the record for the gage located at r = 8 ft. For some shots just one gage was utilized at either r = 6, 10, or 11 ft. Raw data from the wave measurements program are tabulated in Table I.

Dimensionless plots of $\frac{H}{d}$ vs $\frac{d_m}{d}$ at r = 7 ft and r = 8 ft are shown

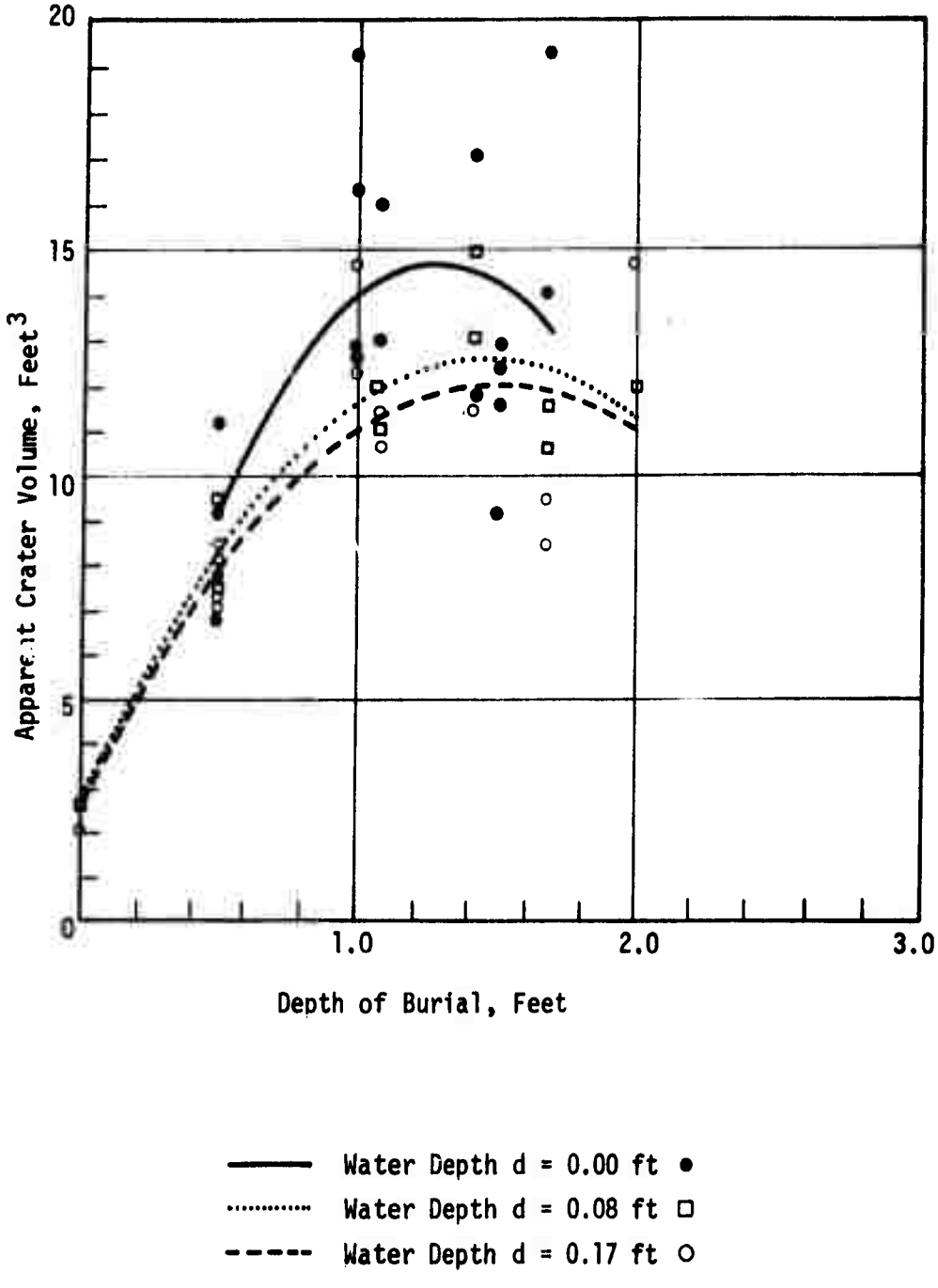


Figure 3. Apparent Crater Volume As A Function of Depth of Burial in Sand For Water Depths of 0.00, 0.08, 0.17 Feet

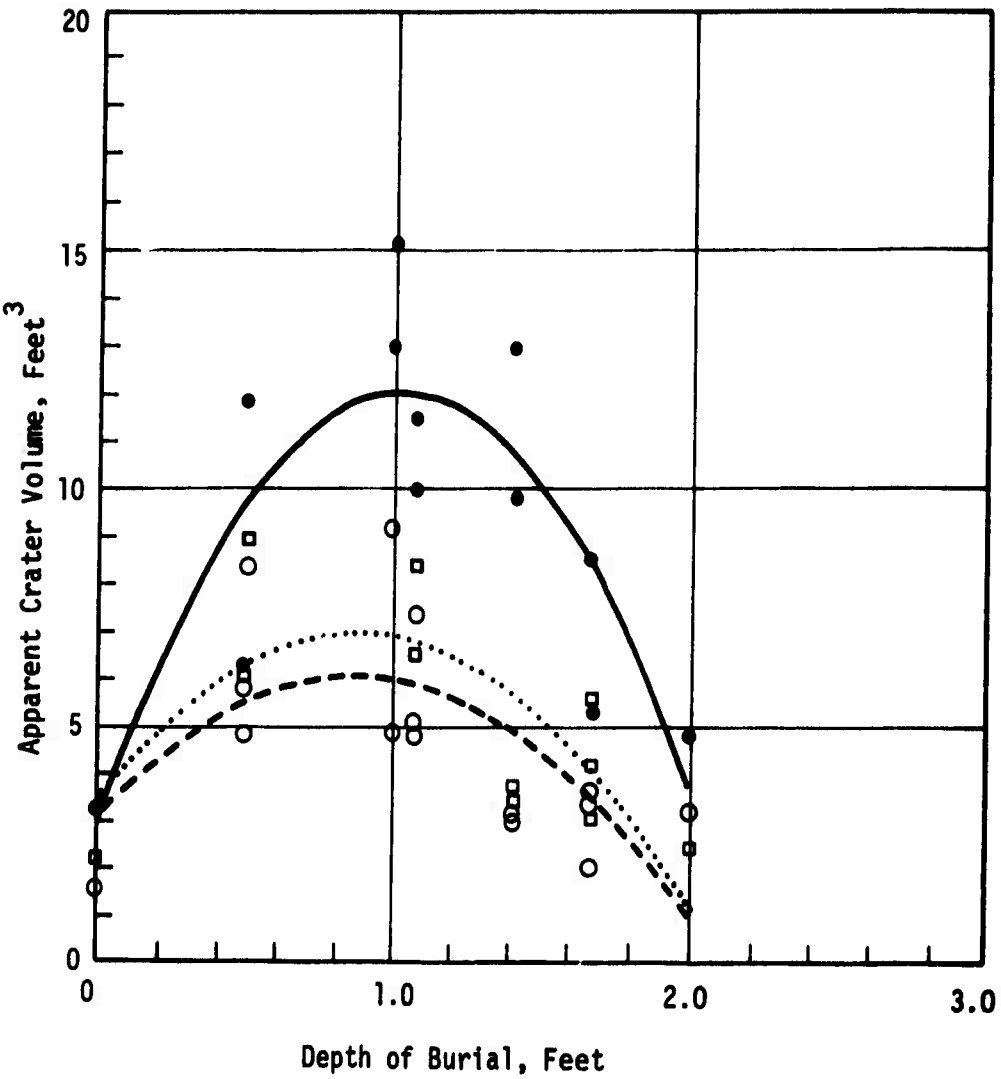


Figure 4. Apparent Crater Volume As A function of Depth of Burial in Sand For Water Depths of 0.33, 0.67, 1.00 Feet

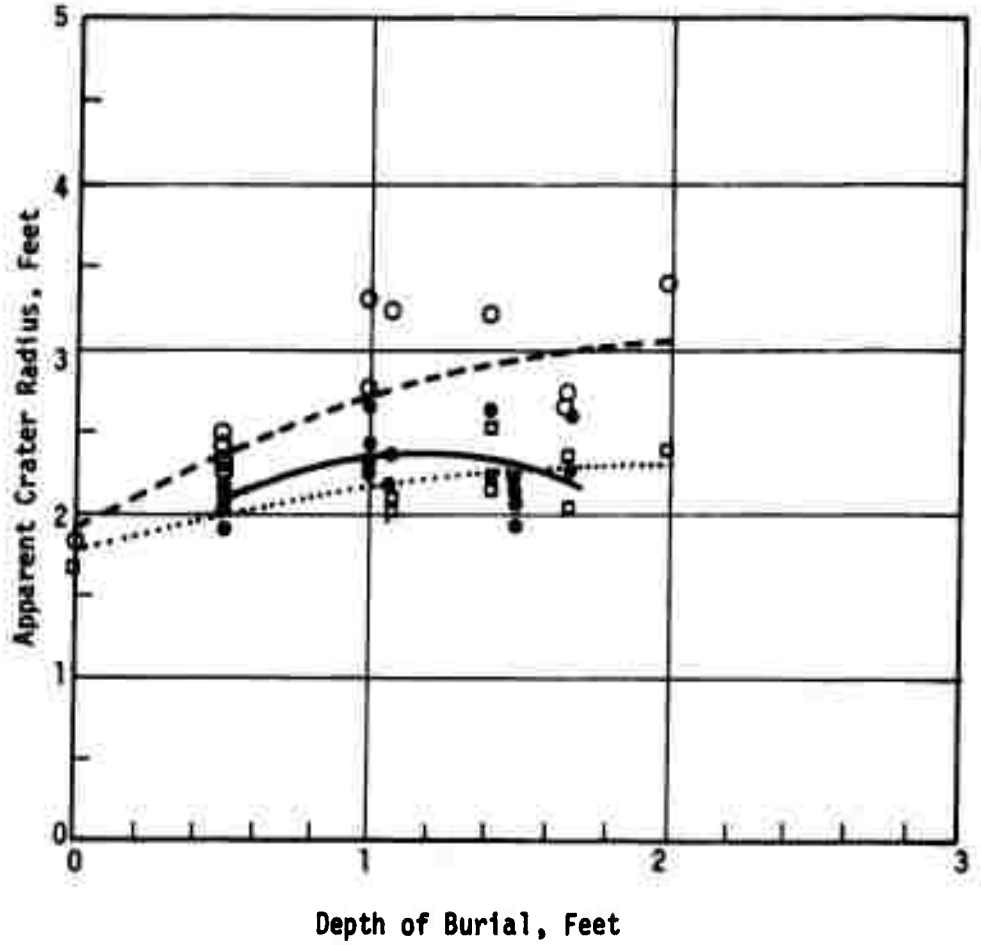


Figure 5. Apparent Crater Radius As A Function of Depth of Burial in Sand For Water Depths of 0.00, 0.08, 0.17 Feet

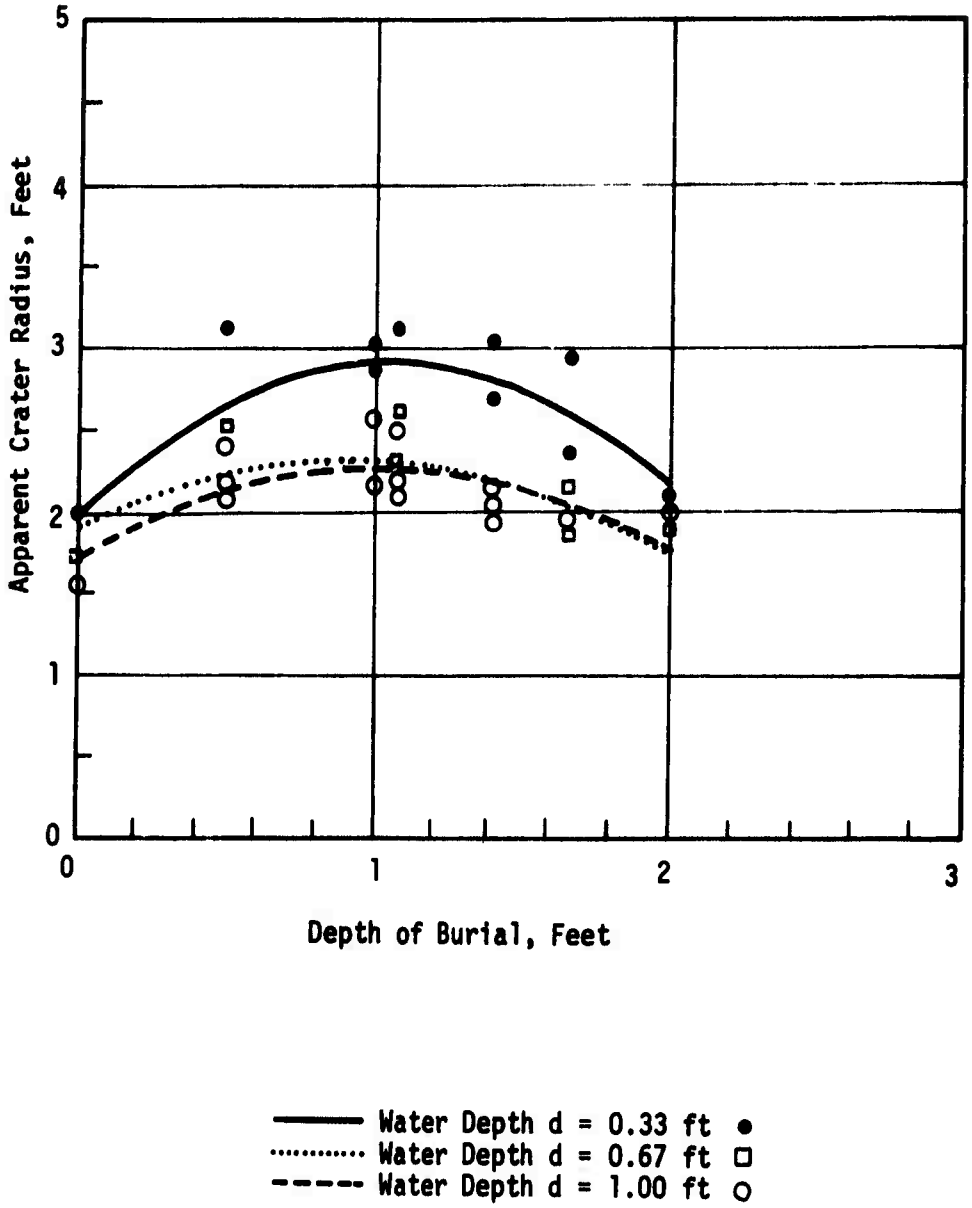


Figure 6. Apparent Crater Radius As A Function of Depth of Burial in Sand For Water Depths of 0.33, 0.67, 1.00 Feet

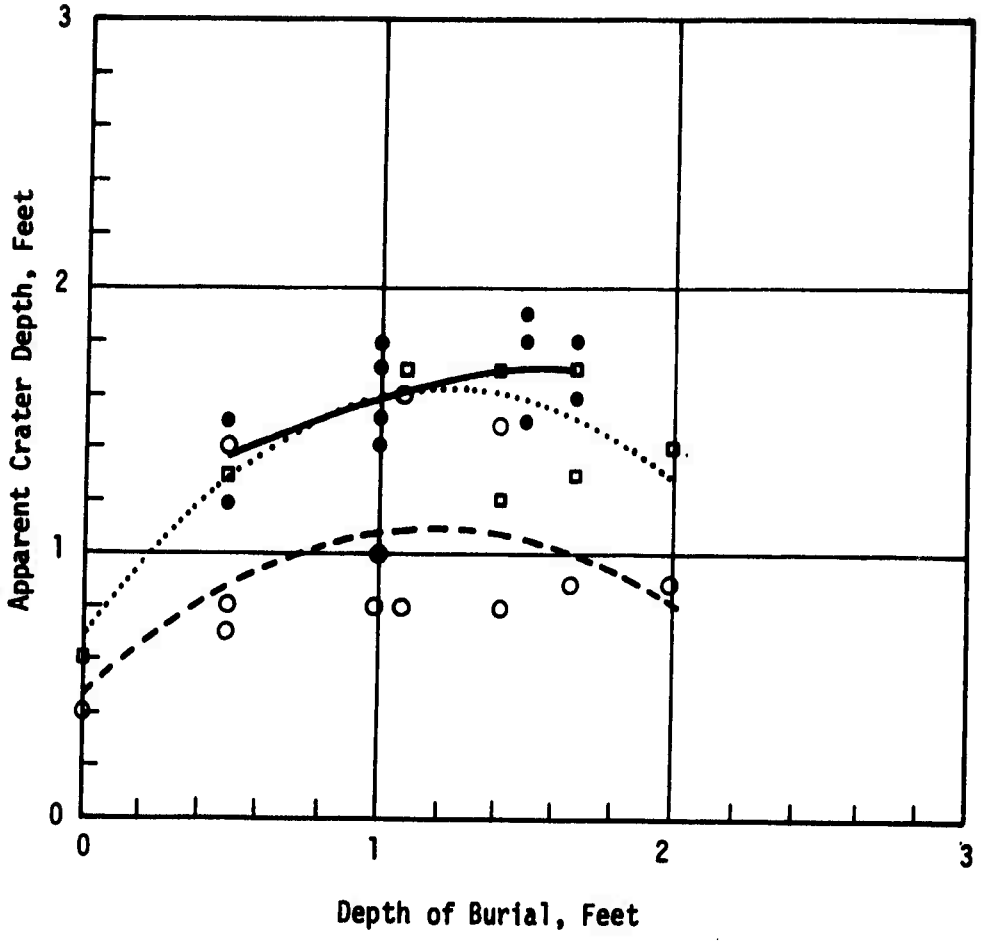


Figure 7. Apparent Crater Depth As A Function of Depth of Burial in Sand For Water Depths of 0.00, 0.08, 0.17 Feet

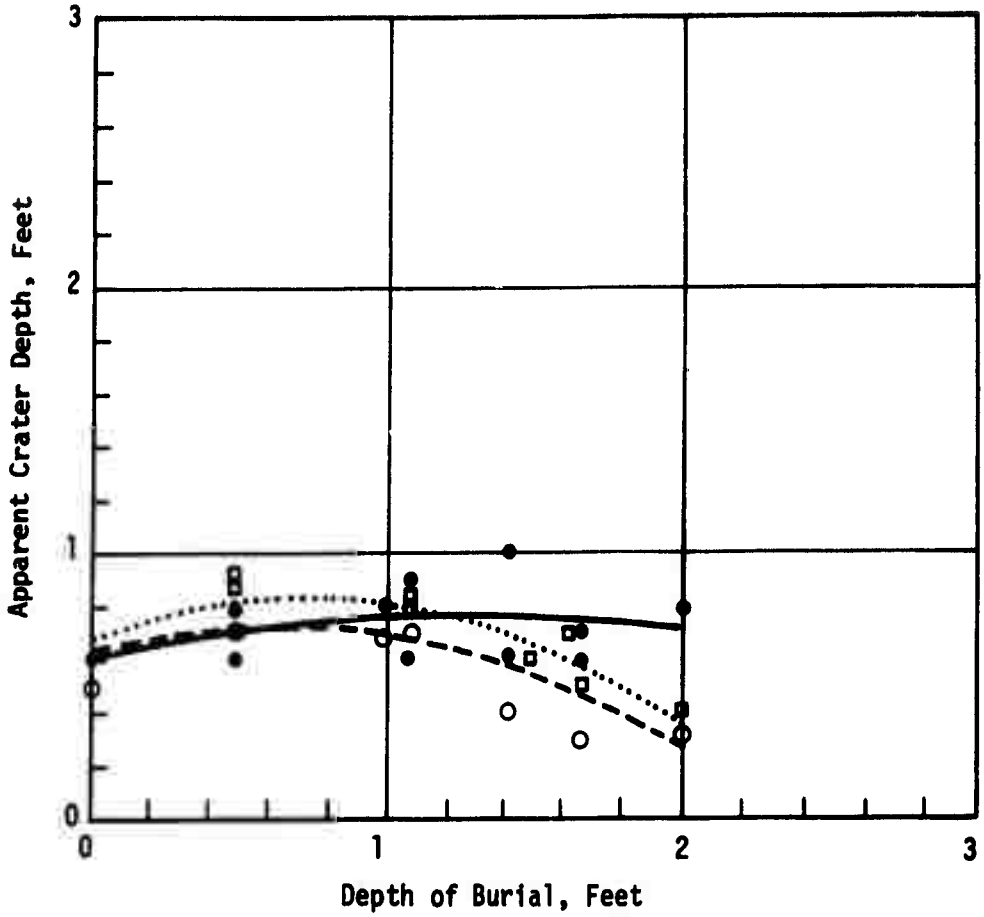


Figure 8. Apparent Crater Depth As A Function of Depth of Burial in Sand For Water Depths of 0.33, 0.67. 1.00 Feet

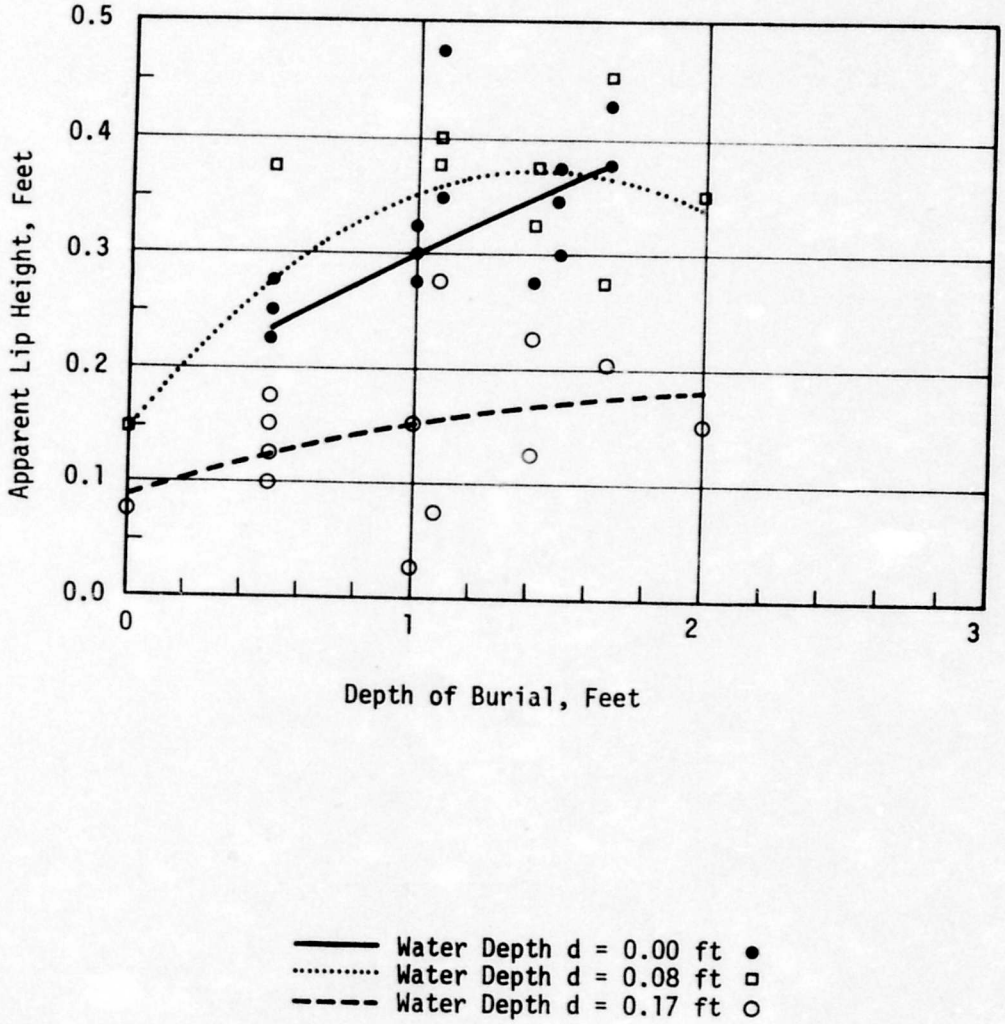


Figure 9. Apparent Lip Height As A Function of Depth of Burial in Sand For Water Depths of 0.00, 0.08, 0.17 Feet

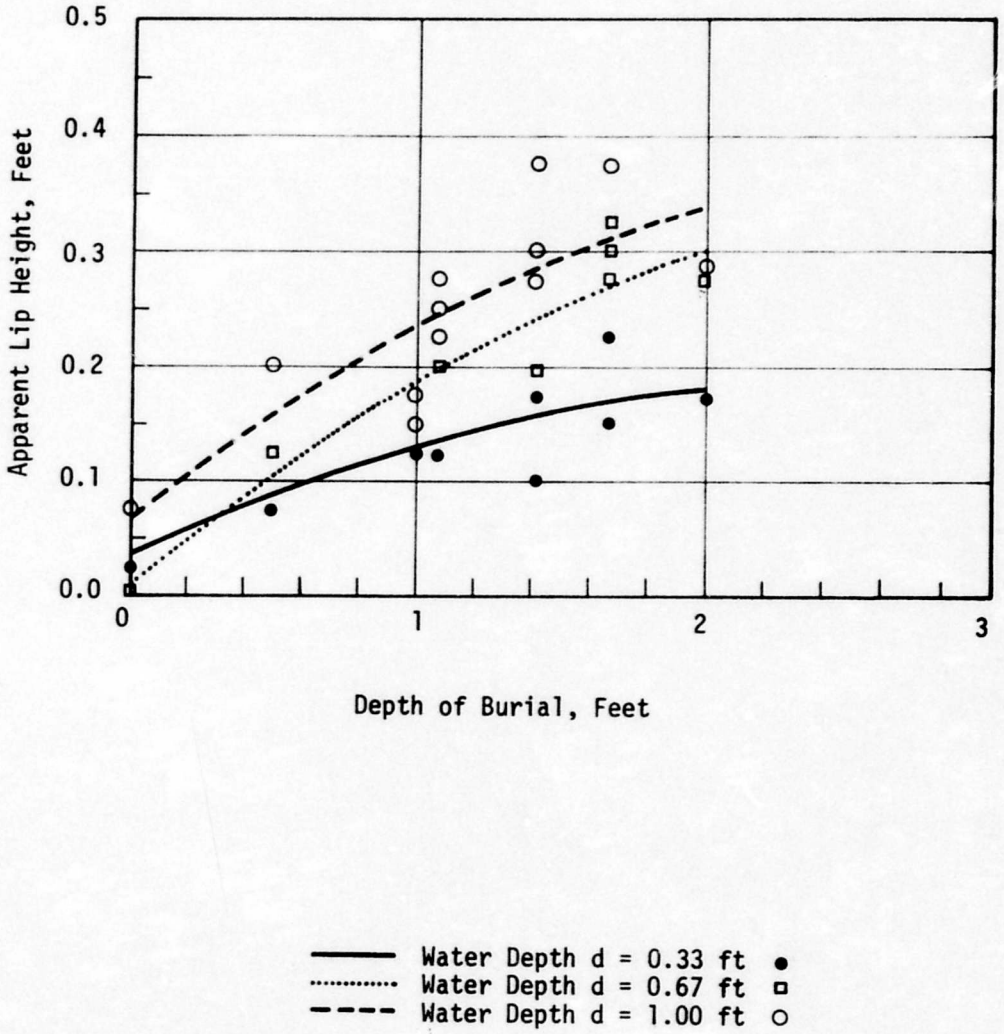


Figure 10. Apparent Lip Height As A function of Depth of Burial in Sand For Water Depths of 0.33, 0.67, 1.00 Feet

EXPLOSION - GENERATED WAVE DATA SHEET

TYPE EXPL. C-4, Spherical DATE 17 Mar 70

WEIGHT EXPL. 1.0 LB SHOT NO. HAD 139

DEPTH OF BURIAL 24 IN

WATER DEPTH AT GZ 8 IN

WATER DEPTH AT WAVE GAGES:

UPPER BEAM (GAGE #1) 8 IN

LOWER BEAM (GAGE #2) 8 IN

WAVE GAGE RANGES:

UPPER BEAM (GAGE #1) 7 FT

LOWER BEAM (GAGE #2) 8 FT

HORIZ. AND VERT. SCALES:

TIME (HORIZ) 1 SEC/CM

WAVE HEIGHT (VERT) 5 IN/CM

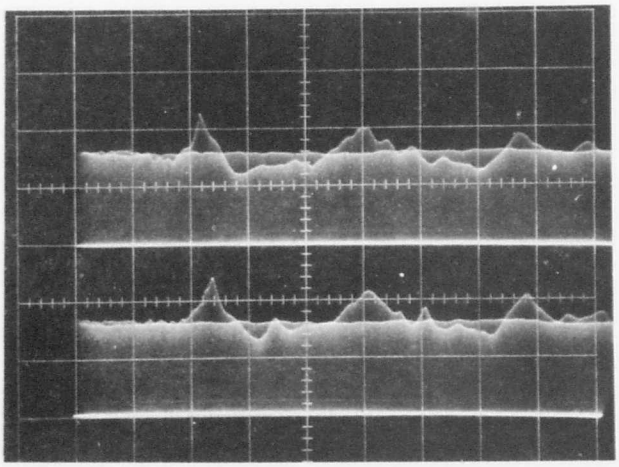

Figure 11. Typical Wave Record

Table I. Maximum Water Wave Data

| Water Depth d (inches) | Depth of Burial in Medium $d_m$ (inches) | Distance from Ground Zero r (inches) | Maximum Wave Height, Crest to Trough H (inches) |
|---|---|---|---|
| 12 | 24 | 120 | 4.1 |
| | | 131 | 3.1 |
| 12 | 20 | 96 | 3.5 |
| 12 | 17 | 96 | 3.9 |
| 12 | 13 | 72 | 4.2 |
| 12 | 6 | 72 | 4.6 |
| 12 | 0 | 120 | 6.3 |
| | | 131 | 6.5 |
| 8 | 24 | 84 | 5.4 |
| | | 96 | 5.3 |
| 8 | 20 | 84 | 3.1 |
| | | 96 | 2.4 |
| 8 | 17 | 84 | 2.6 |
| | | 96 | 2.1 |
| 8 | 17 | 84 | 2.5 |
| | | 96 | 2.1 |
| 8 | 13 | 84 | 3.7 |
| | | 96 | 3.3 |
| 8 | 13 | 84 | 2.7 |
| | | 96 | 2.7 |
| 8 | 6 | 84 | 6.2 |
| | | 96 | 6.1 |
| 8 | 0 | 84 | 8.3 |
| | | 96 | 7.3 |
| 4 | 24 | 84 | 3.0 |
| | | 96 | 3.1 |
| 4 | 20 | 84 | 3.7 |
| | | 96 | 3.6 |
| 4 | 17 | 84 | 3.3 |
| | | 96 | 4.2 |
| 4 | 13 | 84 | 3.7+ |
| | | 96 | 3.0+ |
| 4 | 6 | 84 | 3.2 |
| | | 96 | 2.6 |
| 4 | 0 | 84 | 2.7 |
| | | 96 | 2.6 |
| 2 | 0 | 84 | 3.2 |
| | | 96 | 2.0 |

in Figures 12 and 13, respectively. The maximum wave height, H, is measured from the maximum crest to the succeeding trough. These plots indicate that for a constant water depth, d, the maximum wave height varies cyclically with depth of burial in the medium, $d_m$. Maximum wave heights are generated when the charge is positioned at the water-sand interface. The wave height decreases to a minimum at $\frac{d_m}{d} \approx 2$, then increases to a second maximum at $\frac{d_m}{d} \approx 4$, and then decreases again, probably to a second minimum. The phenomena of these two maxima were also observed for waves generated by charges detonated in the water layer[2]. The charge position for the first maximum was called the "upper critical depth" and the position for the second was called the "lower critical depth".

Although the wave gages were installed for all the water depths tested, intelligible data were obtained only for d = 4, 8, and 12 inches. For d = 1 and 2 inches, the wave records were erratic and unintelligible because of disturbances created by falling ejecta.

## 4. Analysis of Results

### Underwater Cratering

The equation of similitude for the current series of underwater events was derived from the Pi Theorem of dimensional analysis. This theorem which was first stated formally by Buckingham, asserts that any physical, relationship can be represented by a set of independent, dimensionless parameters consisting of product combinations of the physical quantities concerned[7].

The physical quantities that can influence underwater cratering are: (1) a set of linear dimensions defining the boundaries, (2) certain kinematic

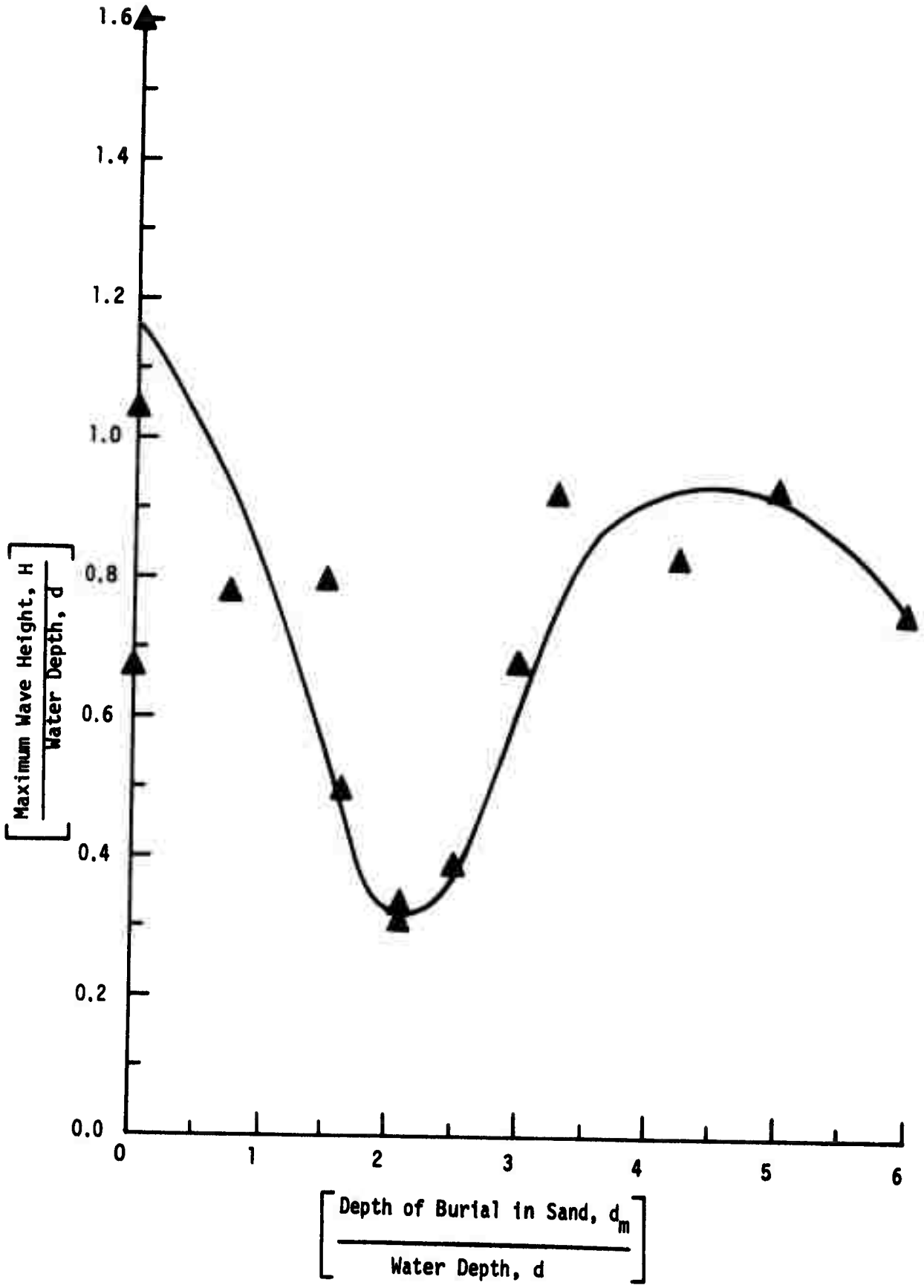


Figure 12. Dimensionless Plot of The Maximum Wave Height At r = 7 Feet As A Function of Depth of Burial in the Medium

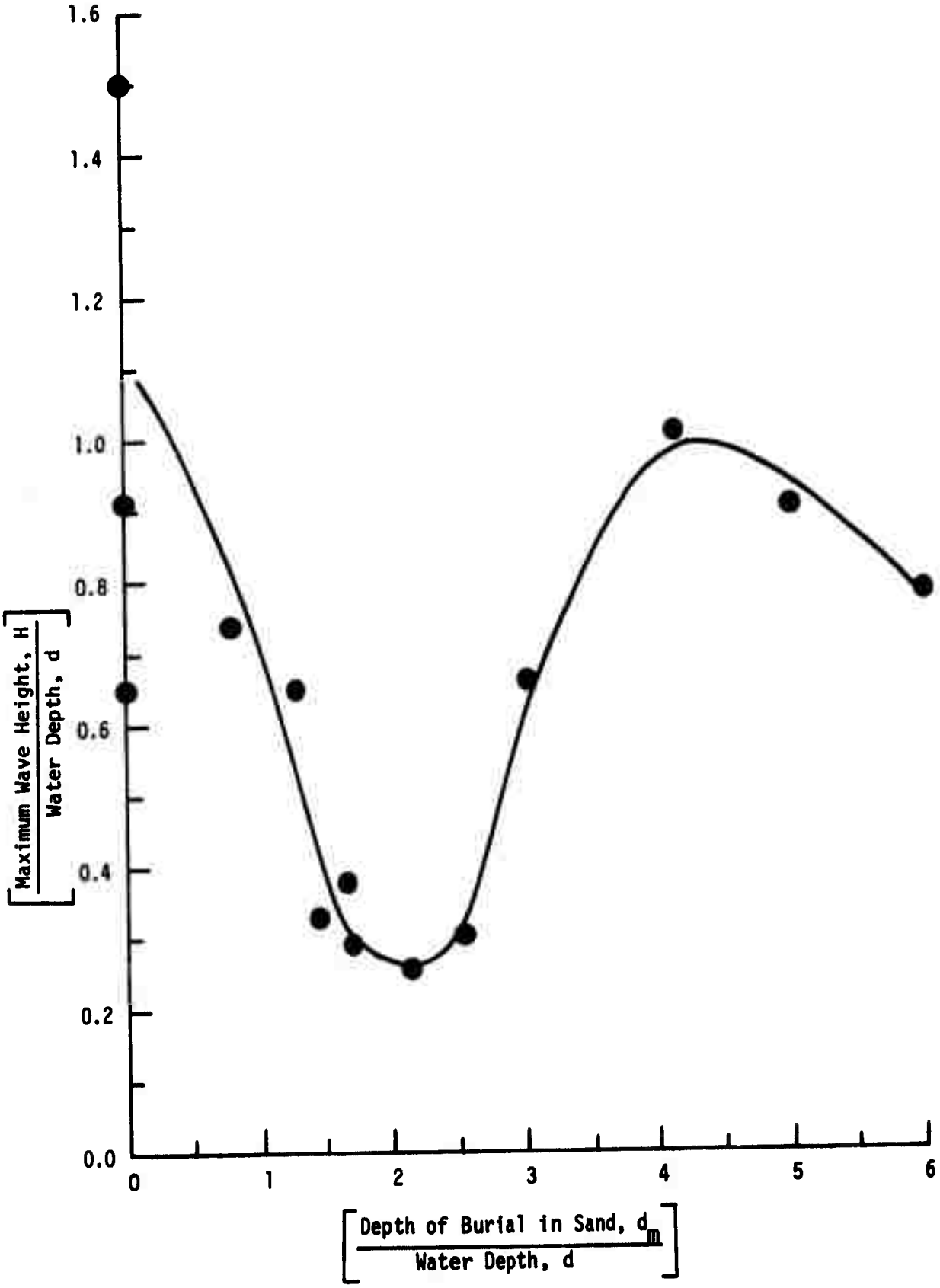


Figure 13. Dimensionless Plot of The Maximum Wave Height At r = 8 Feet As A Function of Depth of Burial in The Medium

and dynamic quantities such as pressure gradients, and (3) the physical properties defining the cratering medium. Accordingly, a general equation for underwater cratering may be written as

$$f(d,\ d_m,\ \rho,\ \rho_m,\ g,\ E,\ L) = 0 \tag{1}$$

where

$d$ = water depth,

$d_m$ = depth of burial in the medium,

$\rho$ = density of water,

$\rho_m$ = density of the medium,

$g$ = gravitational acceleration,

$E$ = explosive energy,

$L$ = a characteristic linear dimension.

From the analysis this equation becomes

$$F(\pi_1,\ \pi_2,\ \pi_3,\ \pi_4) = 0 \tag{2}$$

where

$$\pi_1 = \frac{d}{d_m} \qquad \pi_2 = \frac{\rho g (d_m)^4}{E}$$

$$\pi_3 = \frac{\rho_m g (d_m)^4}{E} \qquad \pi_4 = \frac{L}{d_m}$$

These four dimensionless terms can be combined into the following two independent dimensionless terms:

$$\Pi_1 = \frac{(\rho_m\ g d_m)\ L^3}{E} \qquad \Pi_2 = \frac{(\rho g d)\ L^3}{E} \tag{3}$$

where the expressions in parentheses are the static overburden pressure of the medium and water, respectively.

The final step in the analysis is the determination of the functional relationship between these independent terms based upon physical realities. It is clear that these terms are related by simple addition which yields the term

$$\Pi_3 = (\rho_m g d_m + \rho g d) \frac{L^3}{E} \tag{4}$$

where the expression in parentheses is the confining overburden pressure, z, on the explosive charge. This term can also be written as

$$\Pi_3 = \frac{z L^3}{E} = \frac{\rho g Z L^3}{QW} \tag{5}$$

where

$$Z = d + \left(\frac{\rho_m}{\rho}\right) d_m = d_m \left(\frac{\rho_m}{\rho} + \frac{d}{d_m}\right)$$

is the lithostatic head on the charge expressed as feet of water, Q is the explosive energy released per unit weight of the charge, and W is the total weight of the charge. Since $\rho g/Q$ is constant for this experiment, the law of similitude for the current series of underwater events is

$$\Pi_4 = Z \times \frac{L^3}{W} \tag{6}$$

where L, the characteristic length, is any linear dimension of the crater. Equation (6) can be written as

$$\Pi_4' = Z^{1/3} \cdot \frac{L}{W^{1/3}} = \left[\frac{\rho_m}{\rho} + \frac{d}{d_m}\right]^{1/3} \times \left[L\left(\frac{d_m}{W}\right)^{1/3}\right] \tag{7}$$

or

$$d_m^{1/3} \cdot \frac{L}{W^{1/3}} = f\left(\left[\frac{\rho_m}{\rho} + \frac{d}{d_m}\right]^{1/3}\right) \tag{8}$$

Equation (8) states that changes in crater dimensions are some function of

$\frac{d}{d_m}$, since $\frac{\rho_m}{\rho}$ is a constant for this current underwater cratering experiment. The law of similitude in the form of equation (8) is more convenient to use than the form given by equation (6) since the crater dimension functions are more easily interpreted in terms of the ratio $\frac{d}{d_m}$ than in terms of lithostatic head Z.

Maximum values for crater volume, apparent radius, apparent depth, and lip height with the depth of burial at which they occur for each water depth are tabulated in Tables II and III. These values were obtained from the cratering curves in Figures 3 through 10. The saturated density of the cratering medium, $\rho_m$, was 2.10 grams per cubic centimeter.

Scaled crater volume as a function of $\left(\frac{\rho_m}{\rho} + \frac{d}{d_m}\right)$ is plotted in Figure 14. Scaled crater dimensions as functions of $\left(\frac{\rho_m}{\rho} + \frac{d}{d_m}\right)^{1/3}$ are plotted in Figure 15. A $\frac{d}{d_m}$ scale is included in both figures to facilitate interpretation of these scaling curves. All of these data are also contained in Tables II and III.

Table II. Maximum Crater Volume Data

| Water Depth d (ft) | Max. Volume V ($ft^3$) | Depth of Burial $d_m$ (ft) | $\left[\frac{\rho_m}{\rho} + \frac{d}{d_m}\right]$ | Scaled Volume $V\left(\frac{d_m}{W}\right)$ $Ft^3 x\left(\frac{ft}{lb}\right)$ |
|---|---|---|---|---|
| 0.00 | 14.6 | 1.27 | 2.10 | 18.5 |
| 0.08 | 12.6 | 1.45 | 2.16 | 18.3 |
| 0.17 | 12.1 | 1.50 | 2.21 | 18.2 |
| 0.33 | 12.1 | 1.01 | 2.43 | 12.2 |
| 0.67 | 7.0 | 0.88 | 2.86 | 6.3 |
| 1.00 | 6.0 | 0.88 | 3.24 | 5.3 |

Table III. Maximum Crater Dimension Data

| | Max. Crater Dimension | Depth of Burial Ft | $\left[\frac{\rho_m}{\rho} + \frac{d}{d_m}\right]^{1/3}$ | Scaled Crater Dimension $L \times \left(\frac{d_m}{W}\right)^{1/3}$ |
|---|---|---|---|---|
| **Water depth d = 0.00 ft** | | | | |
| Apparent radius | 2.35 | 1.20 | 1.280 | 2.36 |
| Apparent depth | 1.70 | 1.70 | 1.280 | 2.03 |
| Lip Height | 0.38+ | 1.70+ | 1.280 | 0.45+ |
| **Water depth d = 0.08 ft** | | | | |
| Apparent radius | 2.29 | 1.90 | 1.288 | 2.84 |
| Apparent depth | 1.62 | 1.25 | 1.292 | 1.74 |
| Lip Height | 0.37 | 1.45 | 1.290 | 0.42 |
| **Water depth d = 0.17 ft** | | | | |
| Apparent radius | 3.05 | 2.00 | 1.298 | 3.84 |
| Apparent depth | 1.10 | 1.20 | 1.308 | 1.17 |
| Lip Height | 0.18 | 2.0 + | 1.298- | 0.23+ |
| **Water depth d = 0.33 ft** | | | | |
| Apparent radius | 2.92 | 1.05 | 1.342 | 2.96 |
| Apparent depth | 0.75 | 1.20 | 1.353 | 0.80 |
| Lip height | 0.18+ | 2.0 + | 1.314- | 0.23+ |
| **Water depth = 0.67 ft** | | | | |
| Apparent radius | 2.32 | 0.90 | 1.416 | 2.24 |
| Apparent depth | 0.85 | 0.75 | 1.440 | 0.76 |
| Lip height | 0.30+ | 2.0 + | 1.344- | 0.38+ |
| **Water depth d = 1.00 ft** | | | | |
| Apparent radius | 2.25 | 1.00 | 1.458 | 2.25 |
| Apparent depth | 0.70 | 1.60 | 1.555 | 0.59 |
| Lip Height | 0.34+ | 2.0 + | 1.375- | 0.43+ |

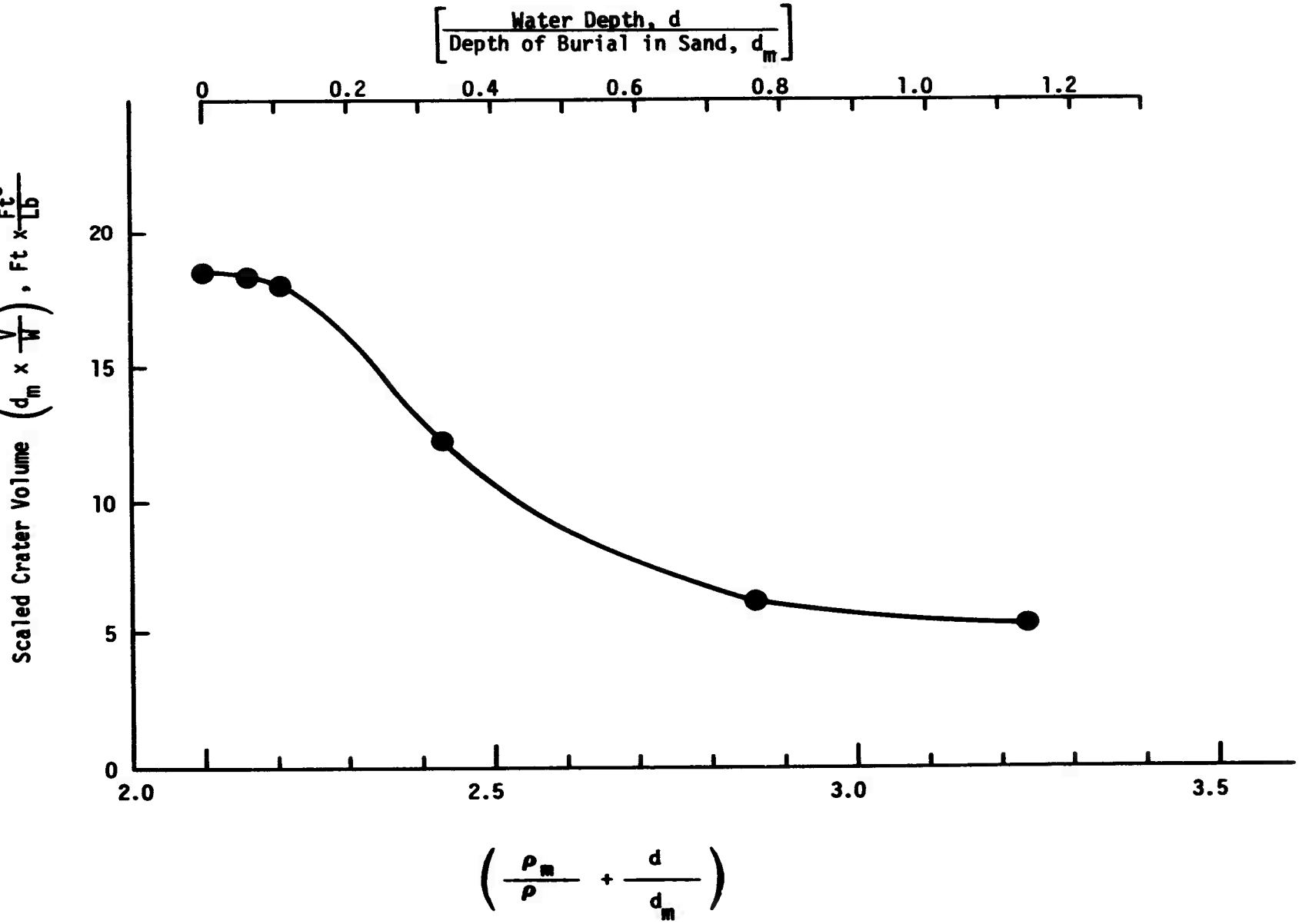


Figure 14. Scaled Crater Volume as a Function of $\frac{d}{d_m}$

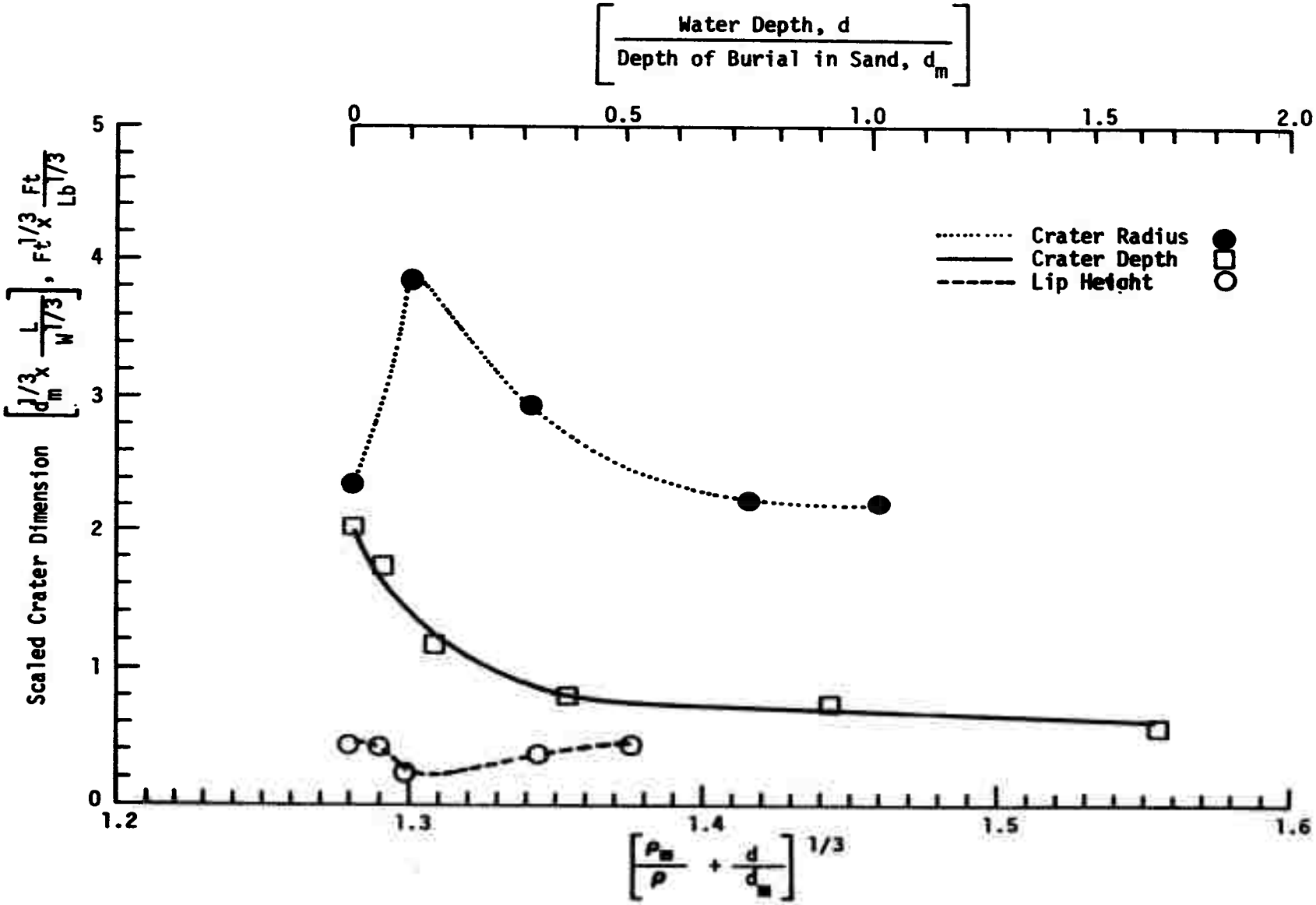


Figure 15. Scaled Crater Dimensions As Functions of $\frac{d}{d_m}$

The scaling curves for the crater radius rises sharply to a maximum at $\frac{d}{d_m} = 0.1$ then decreases to its minimum at $\frac{d}{d_m} = 0.7$. The crater depth is maximum at $\frac{d}{d_m} = 0$, rapidly decreasing to a value near its minimum at $\frac{d}{d_m} = 0.4$, and slowly decreasing thereafter. Unlike the curve for the radius, the curve for the lip height is maximum at $\frac{d}{d_m} = 0$, drops off to its minimum at $\frac{d}{d_m} = 0.1$, then gradually increases to a second maximum.

These curves indicate that for $0 < \frac{d}{d_m} < 0.6$, the crater dimensions are sensitive to small changes in water overburden for a constant depth of burial. The most sensitive region is for $0 < \frac{d}{d_m} < 0.2$ where the crater radius increases sharply, the crater depth decreases sharply, and the lip height decreases as water depth increases. The probable reasons for these phenomena can best be explained by referring to Figure 16 which depicts the change in the crater profiles with water depth for a constant depth of burial $d_m = 20$ inches. For water depths d = 0 inches ($d/d_m = 0.0$) and d = 1 inch ($d/d_m = 0.05$), the crater slopes are relatively steep and the lip height is greater than the water depth. However, for d = 2 inches ($d/d_m = 0.1$), the crater is pan-shaped. This sudden change in crater configuration is caused by the runup of the washback overtopping the crater lip and triggering the failure of the crater slope. This slumping action increases the crater radius and decreases the crater depth. Thus, for $d/d_m < 0.1$, the crater lip is high enough to act as an effective dam against washback runup. But for $d/d_m > 0.1$, overtopping occurs and the crater lip is no longer an effective barrier against the washback. Further increases in water overburden result in decreasing radii and depths although the craters still retain a pan-shaped configuration.

Another effect of the water overburden on underwater cratering can be

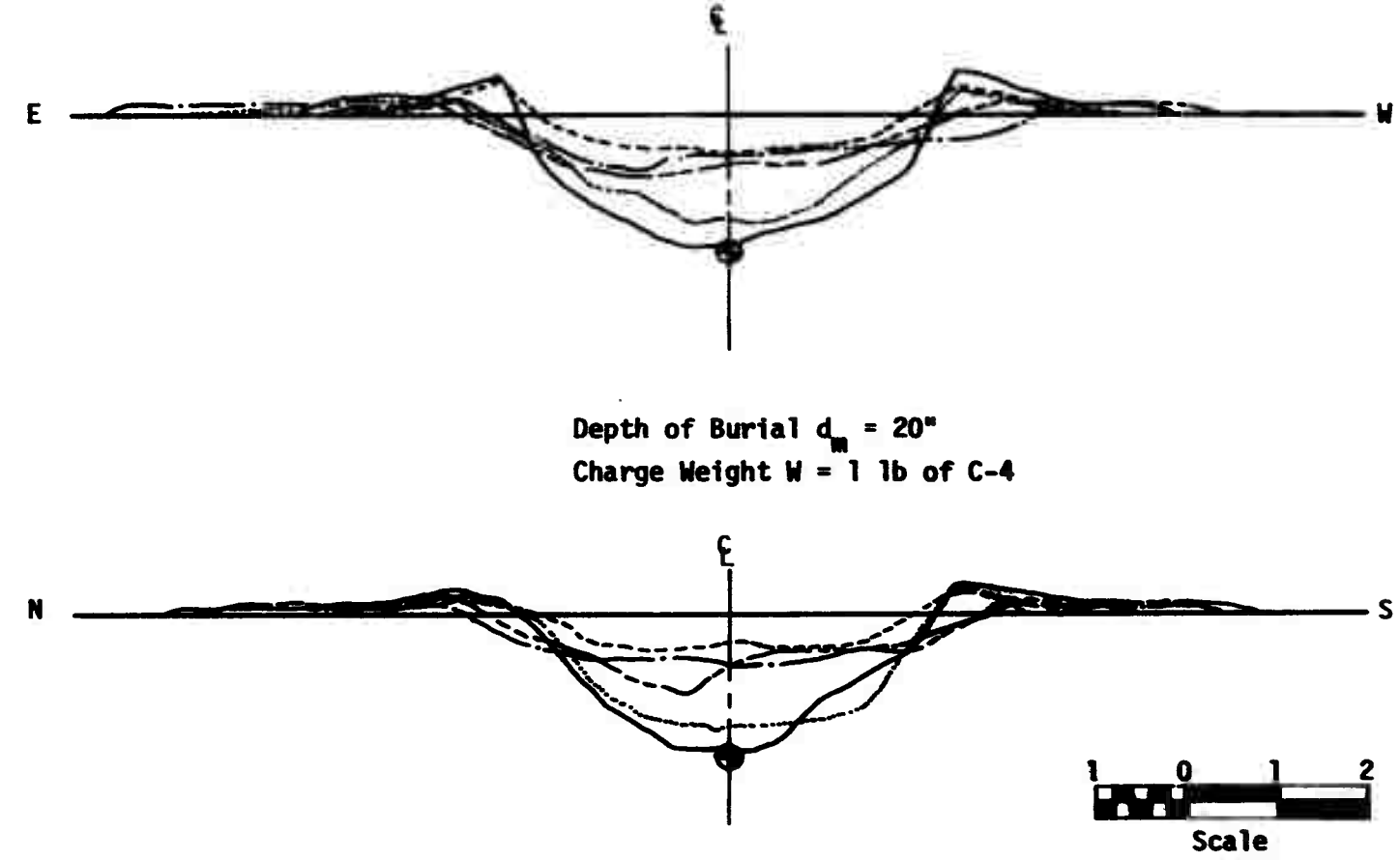


Figure 16. Variation in Crater Geometry With Water Depth For A Constant Depth of Burial in Sand

analyzed with the data presented in Table III. For any water depth, the depths of burial at which the crater radius and crater depth are maximum do not coincide. For water depths of 0.00, 0.08, 0.17, and 1.00 feet, the depths of burial for the maximum radius and depth differ while for water depths of 0.33 and 0.67 feet the depths of burial are nearly the same. Because of the erratic manner by which the depths of burial for maximum crater radius and depth differ with water depth, no relationship is proposed to explain this phenomenon. It is speculated that this difference in the depths of burial is a complicated function of the velocity of the washback, water depth, particle size of the medium, and some strength factor describing the cratering medium.

In comparison, the depths of burial at which the crater radius and crater depth are maximum are usually identical for cratering in a medium without a water overburden. Project ZULU II, Phase I was an experimental cratering series conducted at Bunker 804 (Site 300) in sand with a moisture content of 6 percent with spherical 1-pound C-4 charges[8]. This is the same test facility where the underwater tests were held. Experimental results were that the depth of burial at which the crater radius and depth were maximum was approximately 1.5 feet.

Analysis of Wave Data

A theory for impulsively generated water waves in water of finite depth was developed by Kranzer and Keller[9]. This theory is based on the linear theory of oscillatory surface waves where the wave height is small compared to the water depth and wave length. The solutions developed by this theory are applicable only at distances far removed from the source. The experimental results of the current series cannot be compared with this theory because the conditions for linearity on which the theory is based were not satisfied. First, the wave heights were not small compared to the water

depth and second, the wave measurements were taken as close as possible to the source of disturbance.

Since no adequate theory exists to analyze the wave data, the dimensional analysis, or empirical, approach was taken. Using the Buckingham Pi Theorem and terms previously defined, the following function of dimensionless terms emerges:

$$F\left(\frac{H}{d}, \frac{r}{d}, \frac{d_m}{d}, \frac{d^4 \rho g}{E}, \frac{d^4(\rho_m) g}{E}\right) = 0 \tag{9}$$

The last three terms of the function can be combined into the following two independent dimensionless terms:

$$\Pi_5 = \frac{(\rho g d)\, d^3}{E} \qquad \Pi_6 = \frac{(\rho_m\, g d_m) d^3}{E}$$

where the expressions in parentheses are the static overburden pressure of the water and medium, respectively. These terms are identical in form to $\pi_1$, and $\pi_2$ from the previous section except that the variable L has been replaced by the variable d. Thus, in a manner similar to the previous analysis, the following term is derived:

$$\Pi_7 = \frac{\rho g\, Z\, d^3}{QW} \tag{11}$$

where Z, Q, and W are defined as before. Again, $\rho g/Q$ is constant for this experiment, and the final form of the term is

$$\Pi_8 = \frac{Z d^3}{W} \tag{12}$$

The first two terms of the function in equation (9) can be combined into a single dimensionless term

$$\Pi_9 = \frac{Hr}{d^2}\,. \tag{13}$$

The relationship between $\frac{Hr}{d^2}$ and $\frac{Zd^3}{W}$ is plotted in Figure 17. The equation

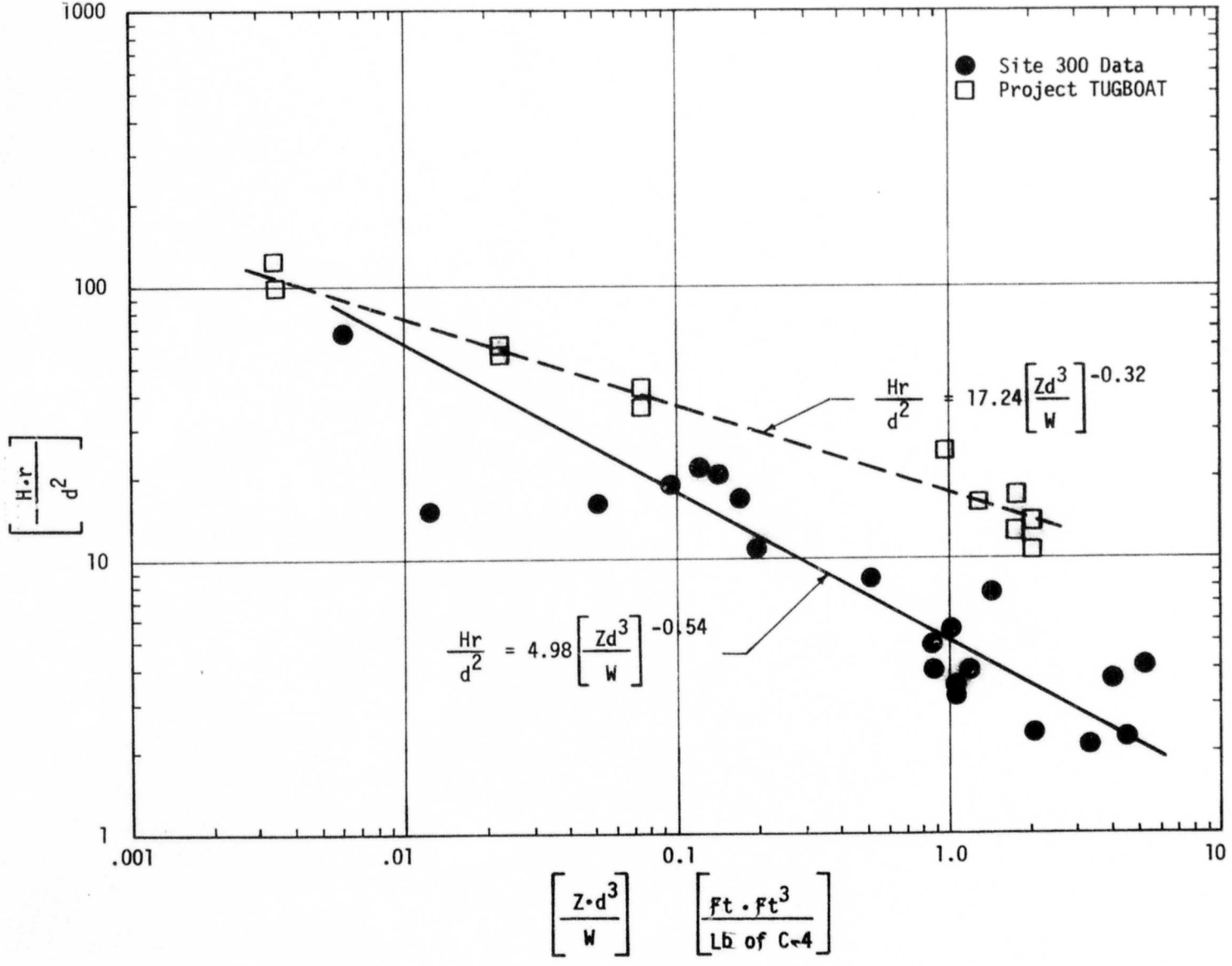


Figure 17. Plot of Empirically Derived Maximum Wave Height Parameters

of the line of least squares fit through the Site 300 wave data is

$$\frac{Hr}{d^2} = 4.98\left[\frac{Zd^3}{W}\right]^{-0.54} \tag{14}$$

Wave data from Project TUGBOAT, a large-scale experiment in coral, are also included for comparison[4]. The empirically derived equation for Site 300 does not fit the TUGBOAT data, due in part to differences in explosive properties and differences in the material properties of sand and coral. There is probably a dependence on scale as well, which is a common factor in modeling work. It should be noted that the TUGBOAT data does plot as a straight line on the axes chosen; only the constant and the exponent need to be adjusted.

## 5. Conclusions

### Underwater Cratering

1. The fundamental parameters for similitude in underwater cratering in a homogeneous, cohesionless medium are the scaled crater dimension

$$L \times \left(\frac{d_m}{W}\right)^{1/3}$$

and the scaled lithostatic pressure on the charge

$$\left(\frac{\rho_m}{\rho} + \frac{d}{d_m}\right)^{1/3}$$

2. An abrupt change in crater dimensions occurs at the critical value of $d/d_m = 0.2$. At this value, the runup of the washback overtops the crater lip and causes a sudden increase in crater radius and a sharp decrease in crater depth.

3. For values of $d/d_m \geq 0.2$, the underwater crater has a flat bottom with gentle side slopes. The crater lip does not protrude above the water surface.

4. For any water depth, the depths of burial at which the crater radius and depth are maximum differ. In comparison, these two depths of burial usually coincide for cratering in a medium without water overburden.

Explosion-Generated Water Waves

1. The relationship which scales the maximum wave generated by the explosion beneath the seabed is

$$\frac{Hr}{d^2} = f\left(\frac{Zd^3}{W}\right)$$

For the Site 300 laboratory model, this relationship is

$$\frac{Hr}{d^2} = 4.98\left[\frac{Zd^3}{W}\right]^{-0.54}$$

2. For any given water depth, the maximum waves will be generated by an explosive placed at the sea bottom (charges above sea bottom not considered). The maximum waves generated by an explosive buried in the seabed occur when the charge is buried in the medium at a depth equal to four times the water depth.

## REFERENCES


1. Davis, L. K. and A. D. Rooke, "High-Explosive Cratering Experiments in Shallow Water," Misc. Paper No. 1-946, Waterways Experiment Station, Vicksburg, Mississippi, December 1968.

2. Van Dorn, W. G., B. LeMehaute, and Li-San Hwang, "Final Report: Handbook of Explosion-Generated Water Waves, Volume I - State of The Art," Tetra Tech Report No. TC-130, Tetra Tech, Incorporated, Pasadena, California, October 1968.

3. Strange, J. N., "Effects of Explosions in Shallow Water," Final Report, Technical Memorandum No. 2-406, Waterways Experiment Station, Vicksburg, Mississippi, April 1955.

4. Day, Walter C., "Project TUGBOAT, Explosive Harbor Excavation in Coral," Technical Report No. 23, U. S. Army Engineer Nuclear Cratering Group, Livermore, California, to be published.

5. Garcia, William J., "Water Waves Produced by Cratering Explosions in Shallow Water," UCRL 50940, LRL, Livermore, California, October, 1970.

6. Bourque, Robert F., "Users Manual for CRATER DATA, A Computer Code for Analyzing Experimental Cratering Tests," NCG/TM-70-15, U. S. Army Engineer Nuclear Cratering Group, Livermore, California, Oct. 1970.

7. Buckingham, Edgar, "Model Experiments and the Forms of Empirical Equations," Transactions, American Society of Mechanical Engineers, Vol. 37, p. 263-296, 1915.

8. Johnson, W. W. and D. L. Nelson, "Project ZULU II, Phase I, Single-Charge Calibration Series," Technical Report No. 3, U. S. Army

References, continued

Engineer Nuclear Cratering Group, Livermore, California, Nov. 1968.

9. Kranzer, Herbert C. and Joseph B. Keller, "Water Waves Produced by Explosions," Journal of Applied Physics, Vol. 30, No. 3, March 1959.

## DISTRIBUTION LIST

Internal

Director

Deputy Director - Military

Deputy Director - Civil

All Division Chiefs

B. Redpath

Michael Florey

Wade Wnuk

Richard Meisinger

Richard Gillespie

Bob Kraut

External

William Garcia - LLL (L-42)

L. K. Davis - WES

A. D. Rooke - WES

Robert Bourque, Stanford Research Institute, Menlo Park, California